

Connection between rotation and miscibility in a two-component Bose-Einstein condensate

Takayuki Shimodaira¹, Tetsuo Kishimoto², and Hiroki Saito¹

¹*Department of Engineering Science, University of Electro-Communications, Tokyo 182-8585, Japan*

²*Center for Frontier Science and Engineering, University of Electro-Communications, Tokyo 182-8585, Japan*

(Dated: January 21, 2020)

A two-component Bose-Einstein condensate rotating in a toroidal trap is investigated. The topological constraint depends on the density distribution of each component along the circumference of the torus, and therefore the quantization condition on the circulation can be controlled by changing the miscibility using the Feshbach resonance. We find that the system exhibits a variety of dynamics depending on the initial angular momentum when the miscibility is changed.

PACS numbers: 03.75.Mn, 03.75.Lm, 67.85.Fg, 67.85.De

I. INTRODUCTION

A Bose-Einstein condensate (BEC) in a toroidal trap [1–4] is an ideal system to study fascinating properties of a superfluid, such as persistent flow [3], symmetry breaking localization [5–8], and various rotating states arising from quantized circulations [9, 10].

The quantization of circulation in superfluids originates from the single-valuedness of the wave function, i.e., the change in the phase of the wave function must be an integer multiple of 2π along a closed path [11, 12]. An angular momentum of a BEC in a toroidal trap is therefore quantized if the density is uniform. However, if a density vanishes at a part of the circumference of the torus, the phase can jump at the density defect [5, 13], and the system is allowed to rotate with an arbitrary circulation.

In the present paper, we consider a system of a two-component BEC rotating in a toroidal trap [14, 15]. Let us consider a situation in which the repulsive interaction separates the two components along the circumference of the torus as illustrated in Fig. 1. Since the closed path along the torus for one component is blocked by the other component, the quantization condition is not imposed on the circulation around the torus, and the system can rotate at an arbitrary frequency. If we decrease the intercomponent repulsion from this initial state, the two components mix, and the density distribution of each component becomes multiply connected, and consequently, the quantization condition is imposed on the circulation along the torus for each component. During this dynamics, the total angular momentum must be conserved. Nontrivial dynamics is thus expected due to the interplay between the change of the quantization condition on the circulation and the angular momentum conservation.

This paper is organized as follows. Section II studies one-dimensional (1D) ring geometry. Section II A gives formulation of the problem. Section II B numerically investigates the stationary states as a function of the intercomponent repulsion for a given angular momentum, and Sec. II C calculates the Bogoliubov spectrum. Section II D compares analytic results with numerical

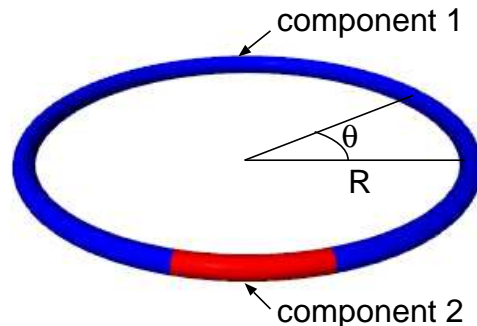


FIG. 1: (color online) Schematic illustration of a phase-separated two-component condensate in a toroidal trap.

ones. Section III demonstrates the dynamics of a two-component Rb BEC in a 3D toroidal trap. Section IV gives conclusions to this study.

II. ONE DIMENSIONAL RING

A. Formulation of the problem

In the mean-field approximation, a two-component BEC in a frame rotating at a frequency Ω around the z axis is described by the Gross-Pitaevskii (GP) equations,

$$i\hbar \frac{\partial \psi_1}{\partial t} = \left(-\frac{\hbar^2 \nabla^2}{2m_1} - \Omega L_z + V_1 + g_{11}|\psi_1|^2 + g_{12}|\psi_2|^2 \right) \psi_1, \quad (1a)$$

$$i\hbar \frac{\partial \psi_2}{\partial t} = \left(-\frac{\hbar^2 \nabla^2}{2m_2} - \Omega L_z + V_2 + g_{22}|\psi_2|^2 + g_{12}|\psi_1|^2 \right) \psi_2, \quad (1b)$$

where ψ_j is the macroscopic wave function for the j th component ($j = 1, 2$) normalized as $\int |\psi_j|^2 d\mathbf{r} = N_j$ with N_j being the number of atoms, m_j is the atomic mass, V_j is the potential, and $L_z = -i\hbar \partial / \partial \theta$ is the z component of the angular momentum operator with $\theta = \arg(x + iy)$.

The interaction parameters are given by

$$g_{jj'} = 2\pi\hbar^2 a_{jj'} \left(m_j^{-1} + m_{j'}^{-1} \right), \quad (2)$$

where $a_{jj'}$ is the s -wave scattering length between atoms in components j and j' . The condition for the phase separation in an infinite system is given by $g_{11}g_{22} < g_{12}^2$ for $g_{jj'} > 0$ [16].

In this section, for simplicity, we reduce the problem to 1D with a periodic boundary condition. We also assume $m_1 = m_2 \equiv m$, $V_1 = V_2$, and $g_{11} = g_{22}$. Assuming that the system is tightly confined in the torus and neglecting excitations in the radial and z directions, we obtain the normalized GP equation as ($j \neq j'$)

$$i \frac{\partial \tilde{\psi}_j}{\partial \tau} = -\frac{1}{2} \frac{\partial^2 \tilde{\psi}_j}{\partial \theta^2} + i\tilde{\Omega} \frac{\partial \tilde{\psi}_j}{\partial \theta} + \tilde{g}_{jj} |\tilde{\psi}_j|^2 \tilde{\psi}_j + \tilde{g}_{jj'} |\tilde{\psi}_{j'}|^2 \tilde{\psi}_j, \quad (3)$$

where the wave function $\tilde{\psi}_j(\theta)$ is normalized as $\int |\tilde{\psi}_j|^2 d\theta = N_j/(N_1 + N_2) \equiv n_j$, $\tau = \hbar t/(mR^2)$, $\tilde{\Omega} = mR^2\Omega/\hbar$, and $\tilde{g}_{jj'} = mR^2 g_{jj'} \rho_{\text{av}}/\hbar^2$ with R being the radius of the torus and ρ_{av} the averaged density.

B. Stationary state with fixed angular momentum

We consider a situation in which a phase separated stationary state in a rotating frame is prepared and then the intercomponent interaction $g_{12} > 0$ is adiabatically decreased, during which the angular momentum of the system is conserved. We therefore seek the stationary state of Eq. (3) for a given angular momentum as a function of g_{12} .

We use the imaginary time propagation method, in which i on the left-hand side of Eq. (3) is replaced by -1 . We add $-\tilde{\mu}_j |\tilde{\psi}_j|^2$ to the right-hand side of Eq. (3) and control $\tilde{\mu}_j$ and $\tilde{\Omega}$ in the imaginary time propagation such that the norm $\int |\tilde{\psi}_j|^2 d\theta = n_j$ in each component and the total angular momentum,

$$\tilde{L} = \tilde{L}_1 + \tilde{L}_2 = -i \sum_{j=1,2} \int \tilde{\psi}_j^* \frac{\partial \tilde{\psi}_j}{\partial \theta} d\theta, \quad (4)$$

are kept constant. The wave function thus converges to the stationary state with given norms n_j and an angular momentum \tilde{L} .

Figure 2 (a) shows the density and phase profiles of the stationary states of Eq. (3), where the populations are $n_1 = 0.9$ and $n_2 = 0.1$ and the total angular momentum is fixed to $\tilde{L} = 0.3$. In Fig. 2, we start from $\tilde{g}_{12} = 1200$ and slowly decrease \tilde{g}_{12} in the imaginary time propagation. At $\tilde{g}_{12} = 1200$ [top panels of Fig. 2 (a)], the two components are phase separated. Component 2 breaks component 1 at $\theta = 0$, where the phase of component 1 changes rapidly. As \tilde{g}_{12} is decreased, the two components are mixed, and the density distribution of each component becomes uniform for $\tilde{g}_{12} \lesssim 980$ [bottom panels of

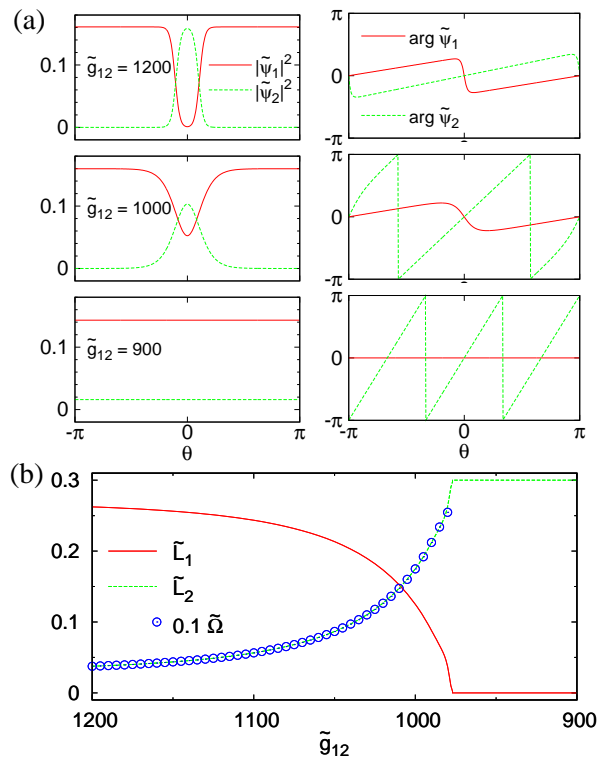


FIG. 2: (color online) (a) Density distributions (left panels) and phase profiles (right panels) of the stationary states of Eq. (3) for $\tilde{g}_{12} = 1200, 1000$, and 900 . (b) Normalized angular momenta \tilde{L}_1 (solid curve), \tilde{L}_2 (dashed curve), and rotation frequency $\tilde{\Omega}$ (circles) of the stationary states as functions of \tilde{g}_{12} . In (a) and (b), $\tilde{g}_{11} = \tilde{g}_{22} = 1000$ and the total angular momentum is fixed to $\tilde{L} = 0.3$. The populations are $n_1 = 0.9$ and $n_2 = 0.1$.

Fig. 2 (a)]. We note that the circulation,

$$\Gamma_j = \frac{1}{2\pi} \int_{-\pi}^{\pi} \frac{\partial \arg \tilde{\psi}_j}{\partial \theta} d\theta, \quad (5)$$

changes due to the constraint of $\tilde{L} = 0.3$ being fixed. As \tilde{g}_{12} is decreased, component 1 goes to the uniform state with $\Gamma_1 = 0$, and in order to maintain $\tilde{L} = 0.3$ the circulation of component 2 increases to $\Gamma_2 = 3$, which satisfies $n_1\Gamma_1 + n_2\Gamma_2 = \tilde{L}$. Thus \tilde{L}_2 increases with a decrease in \tilde{L}_1 as shown by the solid and dashed curves in Fig. 2 (b). The plots in Fig. 2 (b) show the rotation frequency $\tilde{\Omega}$ of the frame in which the density distributions are stationary. We find that $\tilde{\Omega}$ coincides with \tilde{L}_2/n_2 , indicating the rigid-body rotation of component 2 for $\tilde{g}_{12} \lesssim 980$.

Figure 3 shows the case of $\tilde{L} = 0.5$. Unlike in Fig. 2, the dip in $|\tilde{\psi}_1|^2$ persists until $\tilde{g}_{12} = 900$, which is occupied by the localized component 2. The stability of this structure is due to the fact that $\arg \tilde{\psi}_1$ jumps by π at $\theta = 0$ and the stable dark soliton is formed in component 1. As \tilde{g}_{12} is decreased, the tail of $|\tilde{\psi}_2|^2$ spreads and the quantization condition is imposed on the circulation [bottom panels of

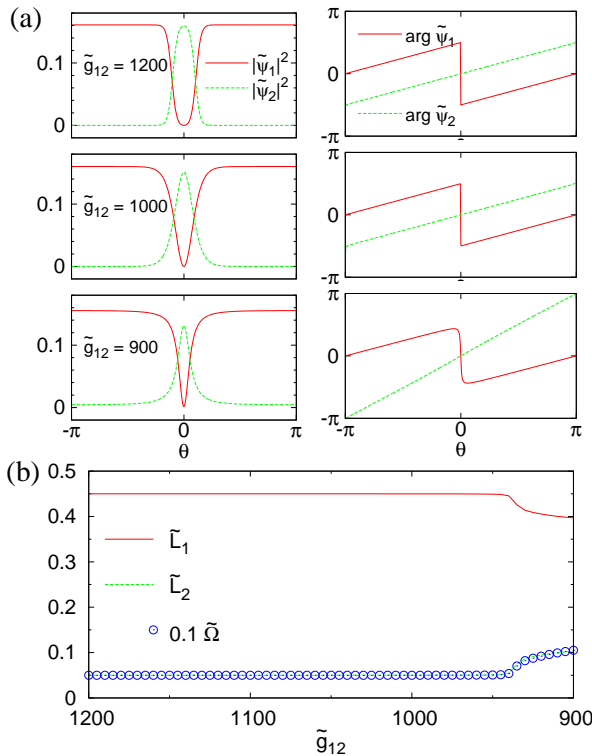


FIG. 3: (color online) (a) Density distributions (left panels) and phase profiles (right panels) of the stationary states of Eq. (3). (b) Normalized angular momenta \tilde{L}_1 (solid curve), \tilde{L}_2 (dashed curve), and rotation frequency $\tilde{\Omega}$ (circles) of the stationary states as functions of \tilde{g}_{12} . The total angular momentum is fixed to $\tilde{L} = 0.5$. The other conditions are the same as those in Fig. 2.

Fig. 3 (a)], which is the reason for the change in \tilde{L}_j at $\tilde{g}_{12} \simeq 950$ in Fig. 3 (b).

Figure 4 shows the case of $\tilde{L} = 0.7$. As \tilde{g}_{12} is decreased, $\tilde{\psi}_1$ goes to a uniform state with circulation $\Gamma_1 = 1$ [bottom panels of Fig. 4 (a)], which has an angular momentum $\tilde{L}_1 = n_1 = 0.9$. As a consequence, \tilde{L}_2 must be $\tilde{L} - \tilde{L}_1 = -0.2$ and therefore Γ_2 becomes $-0.2/n_2 = -2$. Because of $\tilde{L}_2 \simeq n_2 \tilde{\Omega}$, the rotation frequency of the system decreases with \tilde{g}_{12} . This indicates that the rotation of the system slows down, stops, and counterrotates in real time propagation as \tilde{g}_{12} is decreased adiabatically. This interesting behavior is due to the interplay between the quantization of circulation and the angular momentum conservation.

We note that the density distributions in Fig. 2 are exactly the same as those in Fig. 4. This is because the GP equation (3) is invariant under the transformation,

$$\tilde{\psi}_j \rightarrow e^{i\ell\theta} \tilde{\psi}_j^*, \quad (6a)$$

$$\tilde{\Omega} \rightarrow \ell - \tilde{\Omega}, \quad (6b)$$

where ℓ is an integer. By this transformation, the angular

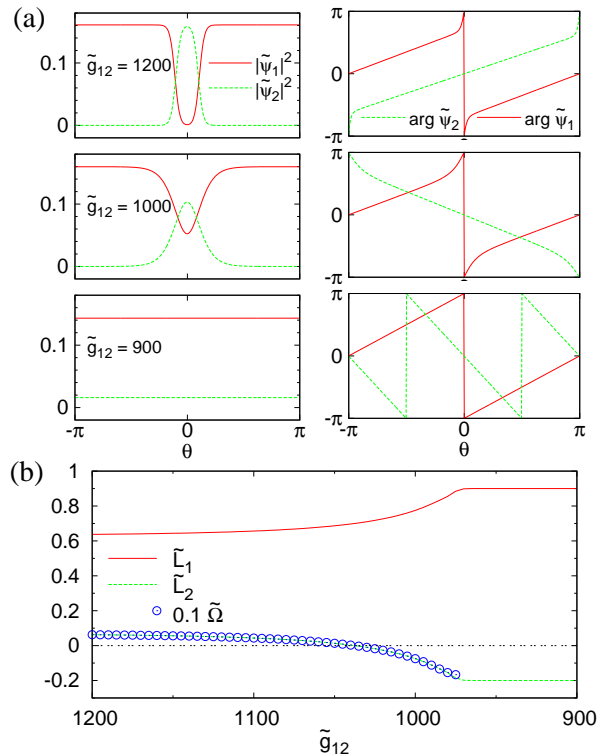


FIG. 4: (color online) (a) Density distributions (left panels) and phase profiles (right panels) of the stationary states of Eq. (3). (b) Normalized angular momenta \tilde{L}_1 (solid curve), \tilde{L}_2 (dashed curve), and rotation frequency $\tilde{\Omega}$ (circles) of the stationary states as functions of \tilde{g}_{12} . The total angular momentum is fixed to $\tilde{L} = 0.7$. The other conditions are the same as those in Fig. 2.

momentum is changed as

$$\tilde{L}_j \rightarrow \ell n_j - \tilde{L}_j. \quad (7)$$

The results in Fig. 4 agree with those obtained from Fig. 2 by the transformation (6) and (7) with $\ell = 1$.

C. Bogoliubov analysis

If the time scale of the change in g_{12} is much longer than the inverse of the lowest excitation frequency, the wave function follows the stationary states shown in Figs. 2-4. In order to find the adiabatic condition, we perform the Bogoliubov analysis.

We separate the wave function as

$$\tilde{\psi}_j(\theta, \tau) = [\Psi_j(\theta) + \delta\psi_j(\theta, \tau)]e^{-i\tilde{\mu}_j\tau}, \quad (8)$$

where Ψ_j is a stationary state of Eq. (3) and ϕ_j is a small deviation. Substituting Eq. (8) with

$$\delta\psi_j(\theta, \tau) = u_j(\theta)e^{-i\tilde{\omega}\tau} + v_j^*(\theta)e^{i\tilde{\omega}\tau} \quad (9)$$

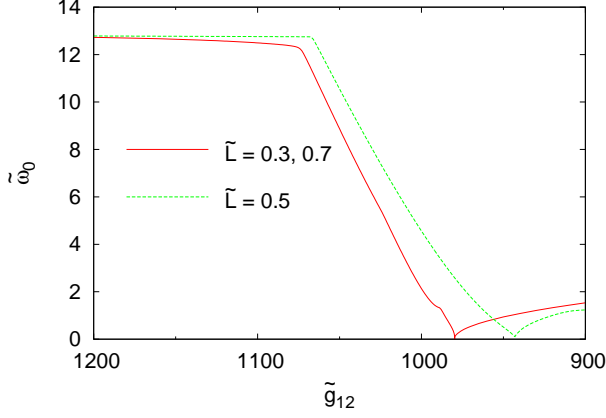


FIG. 5: (color online) The lowest excitation frequency $\tilde{\omega}_0$ for the stationary state with fixed \tilde{L} as a function of \tilde{g}_{12} . For $\tilde{L} = 0.3$ and $\tilde{L} = 0.7$ (solid curve), the excitation frequencies are exactly the same. The parameters are $\tilde{g}_{11} = \tilde{g}_{22} = 1000$, $n_1 = 0.9$, and $n_2 = 0.1$. After the transition to the uniform state in the solid curve, $\tilde{\Omega}$ is fixed.

into Eq. (3) and neglecting the second and higher orders of u_j and v_j , we obtain the Bogoliubov-de Gennes equation ($j \neq j'$),

$$-\frac{1}{2} \frac{\partial^2 u_j}{\partial \theta^2} + i\tilde{\Omega} \frac{\partial u_j}{\partial \theta} + \tilde{g}_{jj}(2|\Psi_j|^2 u_j + \Psi_j^2 v_j) + \tilde{g}_{jj'}(|\Psi_{j'}|^2 u_j + \Psi_j \Psi_{j'}^* u_{j'} + \Psi_j \Psi_{j'} v_{j'}) - \mu_j u_j = \tilde{\omega} u_j, \quad (10a)$$

$$-\frac{1}{2} \frac{\partial^2 v_j}{\partial \theta^2} - i\tilde{\Omega} \frac{\partial v_j}{\partial \theta} + \tilde{g}_{jj}(2|\Psi_j|^2 v_j + \Psi_j^{*2} u_j) + \tilde{g}_{jj'}(|\Psi_{j'}|^2 v_j + \Psi_j^* \Psi_{j'} v_{j'} + \Psi_j^* \Psi_{j'}^* u_{j'}) - \mu_j v_j = -\tilde{\omega} v_j. \quad (10b)$$

We numerically diagonalize Eq. (10).

Figure 5 shows the lowest excitation frequency $\tilde{\omega}_0$ for $\tilde{L} = 0.3, 0.5$, and 0.7 . The excitation frequencies for $\tilde{L} = 0.3$ and 0.7 are exactly the same, since both states are connected to each other by Eqs. (6) and (7). We find that $\tilde{\omega}_0$ decreases with \tilde{g}_{12} and reaches $\tilde{\omega}_0 = 0$, at which the adiabatic condition breaks down. For $\tilde{L} = 0.3$ and 0.7 (solid curve), this point ($\tilde{g}_{12} \simeq 980$) corresponds to the transition to the uniform state, which indicates that the localized state cannot transform to the uniform state adiabatically. For $\tilde{L} = 0.5$ (dashed curve), $\tilde{\omega}_0 = 0$ at $\tilde{g}_{12} \simeq 940$.

For example, let us consider a ^{87}Rb BEC with density 10^{14} cm^{-3} in a ring with radius $10 \mu\text{m}$. In this case the unit of time is $u_t = mR^2/\hbar \simeq 0.14 \text{ s}$. If the typical time scale of change in \tilde{g}_{12} is $1 \text{ s} \sim 10u_t$, the energy gap $\tilde{\omega}_0$ must be $\gtrsim 1$ for the adiabatic condition, and hence \tilde{g}_{12} can be decreased to $\simeq 990$ ($\simeq 960$) for the solid (dashed) curve in Fig. 5.

D. Analysis for rotation frequency

In Sec. II B, we showed that the rotation frequency Ω changes as the intercomponent interaction g_{12} is changed. In this subsection, we derive an analytic expression of the rotation frequency Ω .

We write the wave function as

$$\tilde{\psi}_j(\theta) = \sqrt{\rho_j(\theta)} e^{i\phi_j(\theta)}, \quad (11)$$

where $\rho_j(\theta)$ and $\phi_j(\theta)$ are real functions. We assume that $\rho_2(\theta)$ is localized near $\theta = 0$ and define θ_0 at which ρ_2 decays to zero $\rho_2(\pm\theta_0) \simeq 0$. We also assume that the total density is almost constant, $\rho_1(\theta) + \rho_2(\theta) \simeq (2\pi)^{-1} \equiv \rho_0$, and hence $\rho_1(\theta)$ falls only around $\theta = 0$ and $\rho_1(\theta) \simeq \rho_0$ for $|\theta| > \theta_0$ ($-\pi \leq \theta \leq \pi$). We write the phases as

$$\phi_1(\theta) = \tilde{\Omega}_0 \theta + f(\theta), \quad (12a)$$

$$\phi_2(\theta) = \tilde{\Omega} \theta, \quad (12b)$$

where $\tilde{\Omega}_0$ is a constant determined later. The function $f(\theta)$ changes only around $\theta = 0$ and satisfies $f'(\theta) \simeq 0$ for $|\theta| > \theta_0$. From the single-valuedness of the wave function, Eq. (12a) gives

$$2\pi\tilde{\Omega}_0 + \int_{-\pi}^{\pi} f'(\theta) d\theta = 2\ell\pi, \quad (13)$$

where ℓ is an integer. Since $\rho_2(\theta)$ vanishes for $|\theta| > \theta_0$, there is no constraint on Eq. (12b) for $|\theta| > \theta_0$. Using $\partial\rho_1/\partial t = 0$ and Eq. (3), we find

$$J_1(\theta) - \tilde{\Omega}\rho_1(\theta) = \text{const.}, \quad (14)$$

where J_j is the flux given by

$$J_j(\theta) = \rho_j(\theta)\phi_j'(\theta). \quad (15)$$

From Eqs. (12b), (14), and (15), we obtain

$$f'(\theta) = -(\tilde{\Omega} - \tilde{\Omega}_0) \left[\frac{\rho_0}{\rho_1(\theta)} - 1 \right]. \quad (16)$$

The angular momentum of each component in Eq. (4) is rewritten as

$$\begin{aligned} \tilde{L}_1 &= \int_{-\pi}^{\pi} \rho_1(\theta)\phi_1'(\theta) d\theta = \int_{-\pi}^{\pi} \rho_1(\theta) [\tilde{\Omega}_0 + f'(\theta)] \\ &= \tilde{\Omega}_0 - n_2\tilde{\Omega}, \end{aligned} \quad (17a)$$

$$\tilde{L}_2 = n_2\tilde{\Omega}, \quad (17b)$$

where we used Eqs. (12) and (16). Equation (17b) is consistent with the agreement between the solid curves and circles in Figs 2-4. Equation (17) gives

$$\tilde{L} = \tilde{L}_1 + \tilde{L}_2 = \tilde{\Omega}_0. \quad (18)$$

Using Eqs. (13), (16), and (18), we obtain

$$\tilde{\Omega} = \ell + (\tilde{L} - \ell) \left\{ 1 + \frac{2\pi}{\int_{-\pi}^{\pi} \left[\frac{\rho_0}{\rho_1(\theta)} - 1 \right] d\theta} \right\}. \quad (19)$$

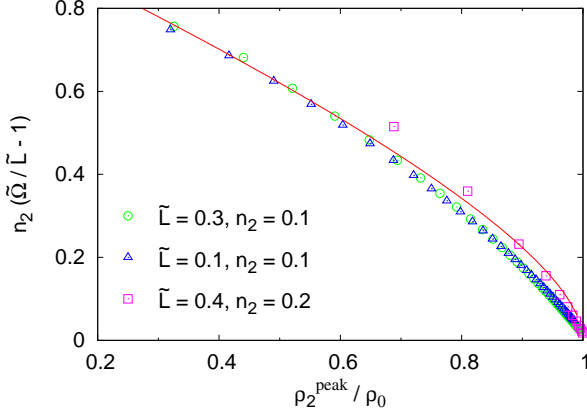


FIG. 6: (color online) Relation between the peak density of component 2 and the rotation frequency for $(\tilde{L}, n_2) = (0.3, 0.1)$ (circles), $(0.1, 0.1)$ (triangles), and $(0.4, 0.2)$ (squares). The solid curve shows Eq. (21).

We assume Gaussian density distributions as

$$\rho_1(\theta) = \rho_0 - \rho_2^{\text{peak}} e^{-\theta^2/\sigma^2}, \quad (20a)$$

$$\rho_2(\theta) = \rho_2^{\text{peak}} e^{-\theta^2/\sigma^2}, \quad (20b)$$

where $\rho_2^{\text{peak}} = n_2/(\sqrt{\pi}\sigma)$ is the peak density of component 2. The Gaussian is assumed to be very narrow, $\sigma \ll 1$, so that the wave functions smoothly connect at $\theta = \pm\pi$. Substituting Eq. (20) into Eq. (19), we obtain

$$\tilde{\Omega} = \ell + (\tilde{L} - \ell) \left[1 + \frac{1}{n_2 \frac{\rho_0}{\rho_2^{\text{peak}}} g_{1/2} \left(\frac{\rho_2^{\text{peak}}}{\rho_0} \right)} \right], \quad (21)$$

where the function $g_{1/2}$ is defined by

$$g_{1/2}(z) = \sum_{k=1}^{\infty} \frac{z^k}{k^{1/2}}. \quad (22)$$

Figure 6 shows $n_2(\tilde{\Omega}/\tilde{L} - 1)$ as a function of $\rho_2^{\text{peak}}/\rho_0 = 2\pi\rho_2^{\text{peak}}$. The plots show the numerical results obtained by solving Eq. (3) and the solid curve shows Eq. (21) with $\ell = 0$, i.e.,

$$n_2 \left(\frac{\tilde{\Omega}}{\tilde{L}} - 1 \right) = \frac{\rho_2^{\text{peak}}}{g_{1/2} \left(\frac{\rho_2^{\text{peak}}}{\rho_0} \right)}. \quad (23)$$

We find that the plots with different parameters fit the universal curve given by Eq. (23). According to Eqs. (6) and (7), numerical results with $\tilde{L} \rightarrow \ell - \tilde{L}$ also agree well with Eq. (21).

III. THREE DIMENSIONAL TOROIDAL TRAP

We perform a numerical calculation of full 3D real-time propagation in a realistic situation. We consider

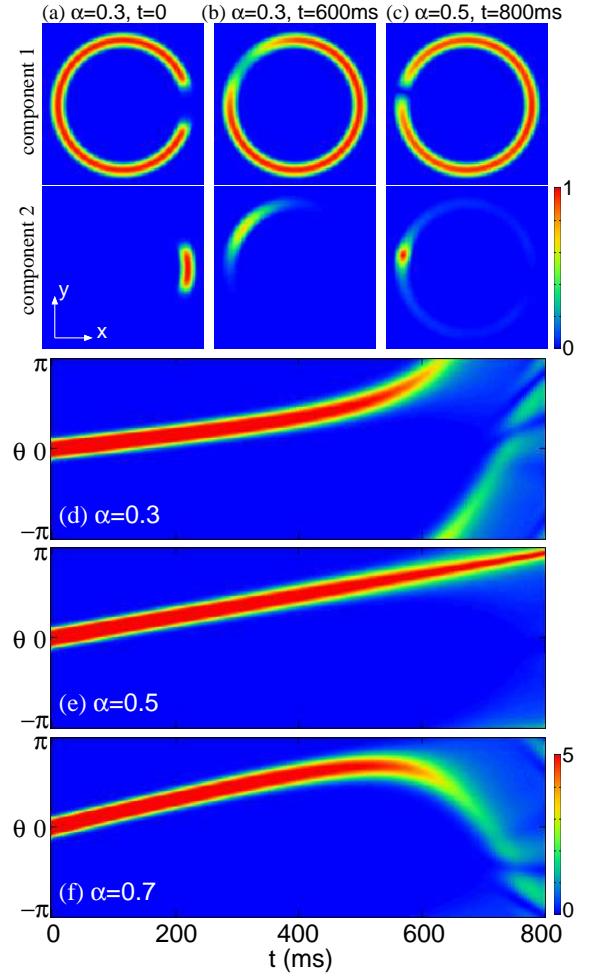


FIG. 7: (color online) Column density profiles $\int |\psi_j|^2 dz$ for (a) $(\alpha, t) = (0.3, 0)$, (b) $(0.3, 60 \text{ ms})$, and (c) $(0.5, 80 \text{ ms})$. The field of view is $25 \times 25 \mu\text{m}$. Density profiles of component 2 at $r_{\perp} = R$ and $z = 0$ for (d) $\alpha = 0.3$, (e) $\alpha = 0.5$, and (f) $\alpha = 0.7$. The density is normalized by N/R^2 in (a)-(c) and by N/R^3 in (d)-(f).

a BEC of ^{87}Rb atoms in the hyperfine states $|F, m_F\rangle = |2, 2\rangle$ and $|2, 1\rangle$, which we refer to as components 1 and 2, respectively. The scattering lengths between component 1 is $a_{11} = a_4$ and that between component 2 is $a_{22} = (3a_2 + 4a_4)/7$, where a_S is the s -wave scattering length between two atoms with total spin S . Their difference is $a_{11} - a_{22} = 3(a_4 - a_2)/7 \simeq 2.98a_B$ with a_B being the Bohr radius, where we used the value measured in Ref. [17]. We therefore use the scattering lengths $a_{11} = 100a_B$ and $a_{22} = (100 - 2.98)a_B$. The intercomponent scattering length a_{12} is assumed to be variable. The number of atoms is $N = N_1 + N_2 = 2 \times 10^5$ with $N_1/N_2 = 9$. We employ a toroidal-shaped trap as

$$V_1 = V_2 = \frac{1}{2}m\omega^2 \left[(r_{\perp} - R)^2 + z^2 \right], \quad (24)$$

with a frequency $\omega = 2\pi \times 1 \text{ kHz}$ and a radius $R = 10 \mu\text{m}$, where $r_{\perp} = (x^2 + y^2)^{1/2}$.

We first prepare the nonrotating ground state $\Psi_j(\mathbf{r})$ for $a_{12} = 100a_B$ by the imaginary-time propagation of Eq. (1), which is phase separated as shown in Fig. 7 (a). We then imprint the phase as $\Psi_j(\mathbf{r})e^{i\alpha\theta}$ with $0 < \theta < 2\pi$ for $j = 1$ and $-\pi < \theta < \pi$ for $j = 2$, where a real parameter α determines the initial angular momentum. In an experiment, such phase imprinting is done by, e.g., spatially modulated laser fields [18]. If α is not an integer, the phase of component 1 (2) jumps at $\theta = 0$ ($\theta = \pi$), at which the density vanishes. Using this initial state, we study the dynamics of the system by solving Eq. (1) in a laboratory frame ($\Omega = 0$) with the pseudospectral method. The intercomponent scattering length is decreased as

$$a_{12}(t) = 100(1 - 0.05t/t_d)a_B \quad (25)$$

with $t_d = 1$ s.

Figures 7 (d)-7 (f) show the dynamics of the density profile of component 2 on the circumference of the torus, $|\psi_2(r_\perp = R, z = 0, t)|^2$. For $t \lesssim 300$ ms, the rotation frequencies are almost constant. At a later time, the rotation of the system accelerates for $\alpha = 0.3$ [Fig. 7 (d)], and reverses for $\alpha = 0.7$ [Fig. 7 (f)]. For $\alpha = 0.5$, the solitonic structure remains until $t = 800$ ms as shown in Fig. 7 (c). These behaviors are consistent with the 1D results in Figs. 2-4. Thus, we have shown that the rotation properties studied for a 1D ring in Sec. II can be observed in a 3D toroidal geometry experimentally.

IV. CONCLUSIONS

We have studied a two-component BEC rotating in a toroidal trap, in which the intercomponent interaction

is controlled. When the two components are phase separated along the circumference of the torus, the system can rotate without topological constraint. As the intercomponent repulsion is decreased and the two components mix, the topological constraint is imposed on the phase of the wave function. Thus, the interplay between the quantization of circulation and the angular momentum conservation exhibits nontrivial phenomena.

We found that as the two components become miscible, the system goes to the states with circulations Γ_j depending on the initial angular momentum L . For a small initial angular momentum (e.g., $L = 0.3N\hbar$), the major component 1 goes to $\Gamma_1 = 0$ while the minor component 2 goes to $\Gamma_2 > 0$, resulting in the acceleration of rotation (Fig. 2). For a larger angular momentum ($L = 0.7N\hbar$), the circulations go to $\Gamma_1 = 1$ and $\Gamma_2 < 0$, and the system counterrotates (Fig. 4). For $L = 0.5N\hbar$, the stable dark soliton is generated (Fig. 3). The Bogoliubov analysis gives the adiabatic condition for the change in the intercomponent repulsion (Fig. 5), and the Gaussian analysis gives the expression of the rotation frequency (Eq. (21) and Fig. 6). The full 3D numerical analysis has shown that the predicted phenomena can be observed in a realistic situation in an experiment.

Acknowledgments

This work was supported by Grants-in-Aid for Scientific Research (No. 20540388 and No. 22340116) from MEXT and Highly Talented Young Researcher under MEXT's Program "Special Coordination Funds for Promoting Science and Technology."

-
- [1] S. Gupta, K. W. Murch, K. L. Moore, T. P. Purdy, and D. M. Stamper-Kurn, *Phys. Rev. Lett.* **95**, 143201 (2005).
 - [2] A. S. Arnold, C. S. Garvie, and E. Riis, *Phys. Rev. A* **73**, 041606 (2006).
 - [3] C. Ryu, M. F. Andersen, P. Cladé, V. Natarajan, K. Helmerson, and W. D. Phillips, *Phys. Rev. Lett.* **99**, 260401 (2007).
 - [4] S. E. Olson, M. L. Terraciano, M. Bashkansky, and F. K. Fatemi, *Phys. Rev. A* **76**, 061404 (2007).
 - [5] L. D. Carr, C. W. Clark, W. P. Reinhardt, *Phys. Rev. A* **62**, 063610 (2000); *Phys. Rev. A* **62**, 063611 (2000).
 - [6] R. Kanamoto, H. Saito, and M. Ueda, *Phys. Rev. A* **67**, 013608 (2003); *Phys. Rev. Lett.* **94**, 090404 (2005); *Phys. Rev. A* **73**, 033611 (2006).
 - [7] G. M. Kavoulakis, *Phys. Rev. A* **67**, 011601 (2003); A. D. Jackson and G. M. Kavoulakis, *Phys. Rev. A* **74**, 065601 (2006).
 - [8] A. Parola, L. Salasnich, R. Rota, and L. Reatto, *Phys. Rev. A* **72**, 063612 (2005).
 - [9] R. Kanamoto, H. Saito, and M. Ueda, *Phys. Rev. A* **68**, 043619 (2003).
 - [10] G. M. Kavoulakis, *Phys. Rev. A* **69**, 023613 (2004).
 - [11] L. Onsager, *Nuovo Cimento Suppl.* **6**, 249 (1949).
 - [12] R. P. Feynman, *Progress in Low Temperature Physics*, vol. 1, ed. C. J. Gorter (North-Holland, Amsterdam, 1955), p17.
 - [13] P. D. Drummond, A. Eleftheriou, K. Huang, and K. V. Kheruntsyan, *Phys. Rev. A* **63**, 053602 (2001).
 - [14] J. Smyrnakis, S. Bargi, G. M. Kavoulakis, M. Magiropoulos, K. Kärkkäinen, and S. M. Reimann, *Phys. Rev. Lett.* **103**, 100404 (2009).
 - [15] F. Malet, G. M. Kavoulakis, and S. M. Reimann, *Phys. Rev. A* **81**, 013630 (2010).
 - [16] See, e.g., C. J. Pethick and H. Smith, *Bose-Einstein Condensation in Dilute Gases* (Cambridge Univ. Press, Cambridge, 2002).
 - [17] A. Widera, F. Gerbier, S. Fölling, T. Gericke, O. Mandel, and I. Bloch, *New J. Phys.* **8**, 152 (2006).
 - [18] M. R. Matthews, B. P. Anderson, P. C. Haljan, D. S. Hall, C. E. Wieman, and E. A. Cornell, *Phys. Rev. Lett.* **83**, 2498 (1999).